

Fast Calculation of Counterparty Credit Exposures and Associated Sensitivities Using Fourier Series Expansion

Gijs Mast* Xiaoyu Shen[†] Fang Fang[‡]

November 22, 2023

Abstract

This paper introduces a novel approach for computing netting-set level and counterparty level exposures, such as Potential Future Exposure (PFE) and Expected Exposure (EE), along with associated sensitivities. The method is essentially an extension of the Fourier-cosine series expansion (COS) method, originally proposed for option pricing. This method can accommodate a broad range of models where the joint distribution of involved risk factors is analytically or semi-analytically tractable. This inclusivity encompasses nearly all CCR models commonly employed in practice. A notable advantage of the COS method is its sustained efficiency, particularly when handling large portfolios. A theoretical error analysis is also provided to justify the method's theoretical stability and accuracy. Various numerical tests are conducted using real-sized portfolios, and the results underscore its potential as a significantly more efficient alternative to the Monte Carlo method for practical usage, particularly applicable to portfolios involving a relatively modest number of risk factors. Furthermore, the observed error convergence rates align closely with the theoretical error analysis.

1 Introduction

Since the 2007–2008 credit crisis, counterparty credit risk (CCR) has been a focal point of banks' risk management for over-the-counter (OTC) derivatives. Risk metrics such as Potential Future Exposure (PFE) and Expected Exposure

*Delft Institute of Applied Mathematics, Delft University of Technology, 2628 CD Delft, the Netherlands (G.L.Mast@tudelft.nl).

[†]Corresponding author, FF Quant Advisory B.V., 3621 ZA Breukelen, the Netherlands (xiaoyu.shen@ffquant.nl).

[‡]Delft Institute of Applied Mathematics, Delft University of Technology, 2628 CD Delft, the Netherlands, and FF Quant Advisory B.V., 3621 ZA Breukelen, the Netherlands (f.fang@tudelft.nl and fang.fang@ffquant.nl).

(EE) are widely used by banks on a daily basis for the quantification and pricing of CCR. Currently, the Monte Carlo (MC) simulation method remains the industry standard for these calculations, and a significantly faster alternative is still elusive. Despite a rich literature on efficient numerical methods for calculating EEs at the trade level, the challenges arise when extending these methods to the portfolio level, such as netting-set and counterparty level. These challenges stem from the diverse range of products within a portfolio and the frequent changes in its composition.

In this paper, we tackle the CCR quantification problem from a novel angle, namely by solving an equivalent problem in the Fourier domain. Specifically, we directly compute the characteristic function (ch.f.) of the total exposure of a portfolio and subsequently reconstruct the cumulative distribution function (CDF) of the total exposure using the well-known Fourier-cosine series expansion (COS) method, originally introduced for option pricing in [2]. The key insight is that the COS method is not limited to option pricing but extends to a broader class of expectation problems. With the obtained CDF of the total exposure, both PFE and EE can be easily determined. The semi-analytical nature of the method allows for a quick calculation of EE sensitivities, and thus, XVA sensitivities.

This approach is applicable whenever the joint density function of the risk factors is known or numerically solvable and when the valuation of each financial product in the portfolio concerns only a few risk factors. In this paper, we illustrate this method for portfolios consisting of liquid interest rate (IR) and foreign exchange (FX) products, driven by three correlated risk factors: a domestic and foreign short rate and the exchange rate of this currency pair. The IR and FX risk factors are assumed to follow the Hull-white model and the Geometric Brownian Motion (GBM) model, respectively. Both netting-set level and counterparty level exposures are covered in this research. As the method is essentially an extension of the COS method from option pricing to CCR risk quantification, we continue to refer to it as the COS method.

Theoretical analysis indicates an exponential error convergence rate of the COS method for computing PFE at the netting-set level. This is further confirmed by the extensive tests we conducted. At the counterparty level, the COS-recovered PFE exhibits algebraic convergence, which aligns with the convergence theory of Fourier series expansions on piecewise continuous functions.

We tested three artificial portfolios of varying sizes. The results of our tests demonstrate that, for a much higher level of accuracy compared to the MC simulation method, the CPU time of the COS method is about 20 – 100 times shorter. This efficiency advantage becomes particularly notable when the portfolio includes a larger number of derivatives. The capacity of MC becomes limited as the portfolio size scales up, a problem that can be expressed as the “computational curse of large portfolios”. As the portfolio size increases, the computational time for MC increases considerably faster than that for the COS method. Thus, the COS method shows potential as a significantly more efficient alternative to the Monte Carlo method for practical usage, particularly for portfolios involving a relatively modest number of risk factors. Note that

the extension of this method to portfolios dependent on many more risk factors and the inclusion of collaterals will be presented in a follow-up paper, wherein we combine efficient dimension-reduction techniques with the COS method to break “the curse of dimensionality”.

The paper is structured as follows. 2 provides an overview of existing methods in the literature. 3 describes the CCR model assumptions adopted in our testing framework. 4 constitutes the main part of this paper, detailing how we extend the COS method to the CCR context: from solving the distribution of the portfolio level exposure to the calculation of risk metrics (such as PFE and EE) and their sensitivities. The error convergence of the COS method is theoretically analyzed in 5. 6 presents numerical test results. We conclude in 7.

2 Literature review

A careful search of recent literature surprisingly reveals a limited number of attempts to address portfolio-level PFE calculations using methods other than MC simulations. While a majority of the literature focuses on fast calculations for exotic or path-dependent derivatives at the deal level or acceleration of MC methods, there is a lack of exploration in alternative methods for portfolio-level PFE calculations.

The single exception known to us is the Approximate Analytical Solution (AAS) method developed in [11, 12]. This method leverages the assumption of normality in risk factors and approximates the log-normal distributions of discounting factors with normal distributions under certain conditions. By making this assumption, explicit expressions can be derived for the EE and PFE of forward rate agreements (FRAs) and European options. The AAS method provides high computational speed at the cost of accuracy, with reported relative differences of up to 10%. It is important to note that the normality assumption of risk and discount factors is quite restrictive and generally holds true only for short periods (see, e.g., [14]).

On the other hand, a significant portion of the existing literature on counterparty credit risk quantification focuses on MC-based methods. These methods utilize MC simulations to calculate credit exposures, particularly for path-dependent derivatives. The nested MC method, which involves simulating risk factor paths and performing nested MC simulations to price exotic derivatives for each scenario, is the most straightforward and robust method. However, the two-layer simulation process is time-consuming due to the large number of required iterations. Various techniques, such as volume reduction in [13] and sample recycling in [3], have been proposed to speed up the nested simulations. Other MC-based method for calculating the credit exposures of path-dependent derivatives include the stochastic grid bundling method in [10], Monte Carlo tree in [19], and Chebyshev polynomial approximation in [5].

In addition to MC-based methods, some researchers have explored the use of neural networks for credit exposure calculations, e.g.[6, 7]. Neural networks serve as function approximators, undergoing training to discern patterns and

relationships between input nodes and the output node(s). The output node(s) may represent either a single position within the overall portfolio or the total portfolio value. Representing a single position offers flexibility when dealing with dynamically changing portfolios, while portraying the total portfolio value is quicker but necessitates retraining for a dynamically evolving portfolio. Although the neural network approach may initially appear distinct from Monte Carlo methods, it is crucial to recognize that the evaluation phase of the neural network approach still depends on estimating portfolio values for randomly sampled risk factor values. Hence, for the purposes of this review, we categorize the neural network approach alongside other MC-based methods.

One disadvantage of MC methods, including the nested MC method and MC-based techniques, is their computational complexity when calculating credit exposures for large portfolios. Since MC methods require pricing all the derivatives in the portfolio for each simulation scenario, the computational burden significantly increases as the portfolio size grows. Furthermore, the calculation of related sensitivities such as EE or XVA sensitivities, where the computation of risk metrics is repeated for multiple times, is even more computationally expensive. This limitation makes MC methods inefficient and time-consuming for large portfolios. In contrast, the proposed COS method does not suffer from this disadvantage.

Importance sampling is a technique that may improve the efficiency of MC methods to estimate the quantile in the tail of the exposure distribution (such as the PFE). However, it is important to note that for large portfolios, there is a significant overhead associated with importance sampling (see, e.g., [4]). The dynamic nature of portfolios and the changing composition of netting sets further complicate the implementation of importance sampling, as a different change of measure may be required for each netting set. These challenges make importance sampling less practical for efficient credit exposure calculations, especially considering the computational complexity and adaptability required for large portfolios.

The limitations of the AAS method and computational challenges of the MC methods for large portfolios are bypassed by the COS method developed in this paper. Unlike existing approaches that focus on individual exotic trades, the COS method directly recovers the probability distribution of the exposure for the entire netting-set or counterparty portfolio. This approach easily covers linear interest rate and foreign exchange products, as well as options for which pricing formulas exist. Additionally, for path-dependent derivatives, some existing methods, such as the Chebyshev polynomial approximation proposed in [5], can be integrated into the COS framework. Thus, the COS method offers a promising alternative for efficient counterparty credit risk quantification in practice.

3 The testing model framework

We consider a simple but typical portfolio subject to three risk factors: interest rates in domestic and foreign currencies, and the FX rate expressed in units of domestic currency per one unit of foreign currency. Regarding the scope of product types, in this article, we choose to include only linear IR and FX products for illustrative purpose. However, the COS method is capable of accommodating all products admitting closed-form pricing formulas, such as IR caps and floors and FX European options. In other words, the scope of products that this method can cover is extensive enough for some real-world applications. In practice, a large portion of the portfolio comprises linear IR and FX products. Nevertheless, as mentioned in 2, for path-dependent derivatives, some existing approximations for pricing can be utilized to allow their inclusion.

To illustrate the core idea of our computational method, we use the Hull–White model for the IR short rates and the geometric Brownian motion (GBM) model for the FX rate. The model framework, while simple, is of practical relevance. Furthermore, we model the risk factors in the real-world measure in a way that we deem appropriate, and price trades in an equivalent martingale measure for the exposure calculations. It is important to note that the COS method is suitable for the general class of affine–jump–diffusion (AJD) models where the joint probability density of the risk factors is tractable (for more discussion, see 4).

3.1 Stochastic processes of the risk factors

A practical approach to using the Hull–White model is to re-represent the short rate $r(t)$ as the sum of the shifted short rate $x(t)$ and a deterministic process $\beta(t)$, which is determined by the initial term structure (see, e.g., [1]). Specifically, we assume the following real-world dynamics for the shifted domestic and foreign short rates, $x_d(t)$ and $x_f(t)$ respectively, and the FX rate $X(t)$:

$$\begin{aligned} dx_d(t) &= -a_d x_d(t)dt + \sigma_d dW_d(t), \\ dx_f(t) &= -a_f x_f(t)dt + \sigma_f dW_f(t), \\ dX(t) &= \mu X(t)dt + \sigma_X X(t)dW_X(t), \end{aligned} \tag{1}$$

with

$$\mathbf{W} = [W_d, W_f, W_X]^T,$$

and

$$d\mathbf{W}d\mathbf{W}^T = \begin{bmatrix} 1 & \rho_{df} & \rho_{dX} \\ \rho_{df} & 1 & \rho_{fX} \\ \rho_{dX} & \rho_{fX} & 1 \end{bmatrix} dt, \tag{2}$$

where ρ_{df} , ρ_{dX} and ρ_{fX} denote the correlations between the standard Brownian motions W_d , W_f , and W_X . The constants a_d and a_f characterize the speed of mean reversion, μ is the drift of the exchange rate and σ_d , σ_f and σ_X denote

the volatility of the respective processes. The initial conditions required by the shifted short rates are $x_d(0) = 0$, $x_f(0) = 0$.

The solutions to the SDEs in 1 are

$$\begin{aligned} x_d(t) &= \sigma_d \int_0^t e^{-a_d(t-s)} dW_d(s), \\ x_f(t) &= \sigma_f \int_0^t e^{-a_f(t-s)} dW_f(s), \\ \log X(t) &= \log X(0) + \left(\mu - \frac{1}{2} \sigma_X^2 \right) t + \sigma_X W_X(t). \end{aligned} \quad (3)$$

Pricing is done in the equivalent risk-neutral measure. The time- t price of a zero coupon bond (ZCB) with maturity T admits a closed-form formula (see, e.g., [1]), i.e.,

$$P_i(t, T) = A_i(t, T) \exp(-B_i(t, T)x_i(t)), \quad (4)$$

with

$$\begin{aligned} B_i(t, T) &= \frac{1}{a_i} \left[1 - e^{-a_i(T-t)} \right], \\ A_i(t, T) &= \frac{P_i^M(0, T)}{P_i^M(0, t)} \exp\left(\frac{1}{2} [U_i(t, T) - U_i(0, T) + U_i(0, t)] \right), \end{aligned} \quad (5)$$

where the subscript i indicates the domestic d or foreign f short rate, $P_i^M(0, T)$ refers to time-0 discount factors, and $U_i(t, T)$ is the time- t conditional variance of $\int_t^T x_i(s)$ given by

$$U_i(t, T) = \frac{\sigma_i^2}{a_i^2} \left(T - t - 2 \frac{1 - e^{-a_i(T-t)}}{a_i} + \frac{1 - e^{-2a_i(T-t)}}{2a_i} \right).$$

All the linear IR and FX products can be priced in closed-form expressions using the ZCB prices, with necessary FX adjustments, i.e., multiplying by X_t to convert the price from the foreign currency to the domestic currency.

3.2 Exposure metrics

The exposure at time t is defined on two levels, i.e., *netting-set level exposure* and *counterparty level exposure*. Mathematically, the exposure of a netting set, i.e., a pool in which all the transactions are covered by a contractual netting agreement, is given by

$$E_t^n = \max(V(\mathbf{X}_t), 0), \quad (6)$$

where $\mathbf{X}_t = [x_d(t), x_f(t), \log X(t)]^T$ is the set of state variables (i.e., certain transformations of the risk factors) that determine the portfolio value and thus the credit exposure, and V is the total Mark-to-Market (MtM) price of the netting set at time t .

If there is only one netting set between two parties, the exposure at the netting-set level is also the exposure at the counterparty level. If there are

multiple netting sets between two parties, the *counterparty level exposure* is the sum of the exposures of all netting sets, i.e.,

$$E_t^c = \sum_{n=1}^N E_t^n = \sum_{n=1}^N \max(V_n(\mathbf{X}_t), 0), \quad (7)$$

where N refers to the number of netting sets between two parties.

PFE can be defined at both the netting-set and counterparty levels. It is a value-at-risk (VaR) metric of E_t , i.e.,

$$\text{PFE}_{\alpha,t} = \inf \{e : \mathbb{P}(E_t \leq e) \geq \alpha\}, \quad (8)$$

where α is the given confidence level, and we use E_t to replace both E_t^c and E_t^n when the calculation concerns both.

The EE at time t is defined as the expectation of the exposure, i.e.,

$$\text{EE} = \mathbb{E}[E_t]. \quad (9)$$

Note that the above definition of EE can be extended to include a discount factor within the expectation operator, i.e., $\mathbb{E}[e^{-\int_0^t r_d(s)ds} E(\mathbf{X}_t)]$. This extension can be applied in the Hull–White–GBM model by adding $\int_0^t x_d(s)ds$ as another state variable, in addition to the shifted short rates and FX rate. The same extension is applicable to other affine jump diffusion models as well.

4 The COS method for CCR quantification

As previously highlighted in 1, our key insight is that the CCR quantification problem can be transformed into an equivalent one in the Fourier domain. This involves solving the continuous Fourier transform of the probability density function, namely the characteristic function (ch.f.), of the total exposure.

4.1 Characteristic function of the exposure

The ch.f. of the exposure, denoted by φ , can be written as integral as below

$$\varphi(\omega) = \mathbb{E}(\exp(i\omega E_t)) = \int \exp(i\omega E(\mathbf{X}_t)) f(\mathbf{X}_t) d\mathbf{X}_t, \quad (10)$$

where i is the imaginary unit, and $f(\mathbf{X}_t)$ represents the joint probability density function of \mathbf{X}_t .

The ch.f. has no closed form solution and is solved by numerical integration in our approach. For ease of numerical integration in the Hull–White–GBM model, we rewrite the state variables as $\mathbf{X}_t = \boldsymbol{\mu}_t + \mathbf{Z}_t$, where $\boldsymbol{\mu}_t$ is the vector collecting the deterministic drifts of the processes in 3, and $\mathbf{Z}_t =$

$[Z_d(t) \ Z_f(t) \ Z_X(t)]^T$, i.e.,

$$\begin{aligned} Z_d(t) &= \int_0^t e^{-a_d(t-s)} dW_d(s), \\ Z_f(t) &= \int_0^t e^{-a_f(t-s)} dW_f(s), \\ Z_X(t) &= W_X(t). \end{aligned} \tag{11}$$

Additionally, we normalize \mathbf{Z}_t as follows: $Z_d(t) = \sigma_{z_d} \hat{Z}_d(t)$, $Z_f(t) = \sigma_{z_f} \hat{Z}_f(t)$, and $Z_X(t) = \sigma_{z_X} \hat{Z}_X(t)$, where \hat{Z}_d , \hat{Z}_f , and \hat{Z}_X are correlated standard normal random variables. By expressing $\hat{\mathbf{Z}}_t = [\hat{Z}_d(t), \hat{Z}_f(t), \hat{Z}_X(t)]^T$ and applying the Cholesky decomposition to the correlation matrix of $\hat{\mathbf{Z}}_t$, we obtain a lower triangular matrix \mathbf{L} such that $\hat{\mathbf{Z}}_t = \mathbf{L} \cdot \tilde{\mathbf{Z}}_t$, where $\tilde{\mathbf{Z}}_t = [\tilde{Z}_d(t), \tilde{Z}_f(t), \tilde{Z}_X(t)]^T$ is a vector of independent standard normally distributed variables.

The ch.f. of the exposure then reads as follows:

$$\begin{aligned} \varphi(\omega) &= \mathbb{E}(\exp(i\omega E(\mathbf{X}_t))), \\ &= \mathbb{E}\left(\exp(i\omega E(\boldsymbol{\mu} + \boldsymbol{\sigma} \mathbf{L} \tilde{\mathbf{Z}}_t))\right), \\ &= \int \exp(i\omega E(\tilde{z}_d, \tilde{z}_f, \tilde{z}_X)) f_N(\tilde{z}_d) f_N(\tilde{z}_f) f_N(\tilde{z}_X) d\tilde{z}_d d\tilde{z}_f d\tilde{z}_X, \end{aligned} \tag{12}$$

where $\boldsymbol{\sigma}$ is a diagonal matrix with the diagonal elements being σ_{z_d} , σ_{z_f} , and σ_{z_X} , and f_N denotes the density function of the standard Normal random variable.

The integral in 12 is evaluated using the Clenshaw–Curtis quadrature method. We define the truncated integration range using the quantile function of the standard normal distribution with a chosen tolerance of error TOL: $[a, b] = [F^{-1}(\text{TOL}), F^{-1}(1 - \text{TOL})]$, where F^{-1} is the inverse of the CDF of the concerned distribution. In our tests, we set $\text{TOL} = 10^{-12}$, and thus, the truncated integration range is symmetric around 0, and covers $1 - 2 \cdot \text{TOL}$ probability mass for each integration variable.

4.2 PFE at the netting–set level

If we consider a large enough truncation range $[a, b]$ of the distribution of the exposure, the Fourier-cosine series expansion of the density function of the exposure E_t^n of a netting set on $[a, b]$ reads

$$f_t^n(e) = C_0/2 + \sum_{k=1}^{+\infty} C_k \cos\left(k\pi \frac{e-a}{b-a}\right)$$

where

$$C_k = \frac{2}{b-a} \int_a^b f_t^n(e) \cos\left(k\pi \frac{e-a}{b-a}\right) de.$$

The COS method proposed in [2] is based on the insight that the Fourier-cosine series coefficients can be directly sampled from the ch.f. as highly accurate

semi-analytical approximations. By applying the COS method to $f_t^n(e)$ and integrating from PDF to CDF, we obtain the COS approximation of the CDF of the exposure E_t^n of a netting set:

$$F_t^n(e) = \mathbb{P}(E_t^n \leq e) \approx F_{t,cos}^n(e) \equiv \frac{A_0}{2}(e-a) + \sum_{k=1}^K A_k \frac{b-a}{k\pi} \sin\left(k\pi \frac{e-a}{b-a}\right), \quad (13)$$

where we use A_k to denote the numerical integration approximation of the COS coefficient F_k (which is directly sampled from the ch.f. and serves as an approximation of C_k):

$$F_k \equiv \frac{2}{b-a} \operatorname{Re} \left\{ \varphi\left(\frac{k\pi}{b-a}\right) \cdot \exp\left(-i \frac{ka\pi}{b-a}\right) \right\}, \quad (14)$$

with Re denoting the real part of a complex number.

There are three sources of errors in 13. The dominating error that governs the rate of convergence is the one originating from the truncation of the expansion terms. The second is the interval truncation error in F_k related with the selection of $[a, b]$, which matters for the accuracy of approximating C_k by F_k . The third error arises from replacing F_k by A_k , whereby the ch.f. values $\varphi\left(\frac{k\pi}{b-a}\right)$ are approximated by numerical integration.

The definition of the exposure of a netting set requires flooring of the portfolio value at 0. Because of that, the Fourier series expansion is subject to the Gibbs phenomenon around the discontinuity at 0. To overcome this issue, instead of directly recovering the distribution of the netting set exposure, we first apply the COS method to recover the distribution of the total MtM price $V(\mathbf{X}_t)$ in the same way as in 13. After that, we can apply the transformation below to obtain the CDF of the netting set exposure:

$$F_{t,cos}^n(e) = \begin{cases} 0 & \text{if } e \leq 0, \\ F_{t,cos}^V(e) & \text{if } e > 0. \end{cases}, \quad (15)$$

where $F_{t,cos}^V(e)$ denotes the COS approximation of the CDF of the total MtM price of the netting set, i.e., $\mathbb{P}(V(\mathbf{X}_t) \leq e)$.

Finally, after the CDF of the netting set exposure is recovered, the PFE can be easily obtained from the CDF by applying a root-searching algorithm on $F_{\text{Netting}}(e) = \alpha$, where α is typically the 97.5%-quantile.

4.3 PFE at the counterparty level

For netting-set level exposure, we could use a transformation, thereby keeping the integrand of the characteristic function smooth and avoiding the Gibbs phenomenon. However, the counterparty level exposure is, by definition, the summation of multiple floored random variables, making the transformation infeasible. On that account, we recover the CDF of the counterparty-level exposure directly via 13. The literature includes two groups of methods to reduce the Gibbs phenomenon resulting from discontinuities in the functions to

be approximated via Fourier expansions: spectral filters and the time-domain equivalent physical mollifiers. Since spectral filters work in the Fourier domain, they are easily implemented, ensuring an improved convergence rate without extra computational costs, see, e.g., [18].

For the counterparty level exposure E_t^c involving multiple netting sets, the Fourier series expansion of the CDF of E_t^c , adjusted by a spectral filter, reads

$$F_t^c(e) = \mathbb{P}(E_t^c \leq e) \approx F_{t,\cos}^c(e) \equiv \frac{A_0}{2}(e-a) + \sum_{k=1}^K A_k \sigma\left(\frac{k}{K}\right) \frac{b-a}{k\pi} \sin\left(k\pi \frac{e-a}{b-a}\right). \quad (16)$$

where the spectral filter $\sigma(\cdot)$ is a real and even function supported on $[-1, 1]$ (see, e.g., [20] and [8]).

Remark 1. *The approximation above contains the same sources of error seen in the approximation without a filter. However, due to the Gibbs phenomenon, the convergence rate is dominated by the order of the spectral filter. The theoretical convergence rate is discussed in 5.*

In the same way as before, the PFE is acquired via a root-finding algorithm on the difference between the approximated CDF and the 97.5%-quantile.

4.4 EE and EE sensitivities

Below, we demonstrate how to evaluate EE and its sensitivities in our framework.

Using a change of variables, 9 transforms to

$$EE = \int_{\mathbb{D}} \max(v_t, 0) f_V(v_t) dv_t, \quad (17)$$

where $f_V(v_t)$ denotes the density of $V(\mathbf{X}_t)$. We already have the Fourier-cosine expression for $f_V(v_t)$ while solving the distribution of the netting-set level exposure (see 4.2). Plugging the cosine series expansion of $f_V(v_t)$ into the 17 and exchanging the order of integration and summation, we find the following expression for EE:

$$EE \approx \frac{A_0}{2} (\max(b, 0)^2 - \max(a, 0)^2) + \sum_{k=1}^K A_k \frac{b-a}{k\pi} \left[\max(b, 0) \sin\left(k\pi \frac{\max(b, 0) - a}{b-a}\right) - \max(a, 0) \sin\left(k\pi \frac{\max(a, 0) - a}{b-a}\right) + \frac{b-a}{k\pi} \left(\cos\left(k\pi \frac{\max(b, 0) - a}{b-a}\right) - \cos\left(k\pi \frac{\max(a, 0) - a}{b-a}\right) \right) \right]. \quad (18)$$

Remark 2. *The above formula considers netting-set level exposure. In the case of counterparty level exposure, the EE sensitivities, by definition, can be expressed as the sum of the EE sensitivities of all the netting sets with respect to the counterparty.*

The EE sensitivities are defined as the partial derivatives of the EE with respect to the values of the risk factors at $t = 0$. E.g., the EE sensitivity with respect to the domestic short rate is as follows:

$$\frac{\partial \text{EE}}{\partial x_{d,0}} = \frac{\partial A_0}{\partial x_{d,0}} \frac{(\max(b, 0)^2 - \max(a, 0)^2)}{2} + \sum_{k=1}^K \frac{\partial A_K}{\partial x_{d,0}} \frac{b - a}{k\pi} [\dots], \quad (19)$$

where \dots refer to terms inside the brackets $[\]$ in 18. Note that the partial derivatives only matter for the coefficients A_k .

There is no analytical solution for $\frac{\partial A_K}{\partial x_{d,0}}$ and we resort to the shock-and-revalue method that is widely used in practice. That is, we shift up the initial value of the risk factor by 1 basis point (BP) and revalue the EE.

4.5 The truncation range

The size of the COS truncation range $[a, b]$ influences the accuracy of the retrieved CDF. If the truncation range is too narrow, the domain of the density function that is of our interest will not be well covered. Whenever the range is too wide, a large number of cosine series terms are needed to capture the important basis functions, or in other words important “frequencies” in the Fourier domain.

For the truncation range $[a, b]$, we propose the following rule-of-thumb:

$$[a, b] := [\mu_E \pm L \cdot \sigma_E] \text{ with } L = 8, \quad (20)$$

where μ_E is the first moment of the exposure and σ_E is the standard deviation. μ_E and σ_E can be obtained using the same numerical integration method as for the ch.f., i.e.,

$$\mathbb{E}[E^k] = \int E^k(\tilde{z}_d, \tilde{z}_f, \tilde{z}_X) f(\tilde{z}_d) f(\tilde{z}_f) f(\tilde{z}_X) d\tilde{z}_d d\tilde{z}_f d\tilde{z}_X. \quad (21)$$

Particularly, note that for counterparty level exposure, we can simply let $a = 0$ since the exposure is by definition floored at 0; and that for the netting set exposure, we do need to find a proper a to use the transformation 15. Thus effectively we only need to solve b for counterparty level exposure.

Remark 3. *The numerical integration for the moments is significantly less computationally expensive than that for the ch.f., because it avoids the need to calculate the complex exponent. Additionally, it requires only a few quadrature points since the truncation range is an approximation that requires lower accuracy.*

4.6 Advantages in computational complexity

For a large class of models, e.g., the affine jump diffusion models, the joint probability density function of the risk factors $f(\mathbf{X}_t)$ is either analytically or semi-analytically tractable. In light of this, the COS method for counterparty credit exposure can be summarized as below:

- Determine the joint density function of the state variables that characterize the exposure distribution, i.e., $f(\mathbf{X}_t)$.
- Evaluate the ch.f. φ of the MtM of the portfolio at netting-set level or the exposure at counterparty level via numerical integration.
- Apply the COS method to recover the distribution of the exposure at the portfolio level in a one-step semi-analytical calculation, from which PFEs and EEs can be easily obtained.

The COS method provides big computational advantages over MC methods as the size of the portfolio grows. Our numerical tests in 6 confirm that it is particularly powerful in this regard, i.e., the computational time increases by a very limited amount as the size of the testing portfolio grows from 100 trades to 10,000 trades. To understand this effect, first note that the computational complexity of the COS method is dominated by the numerical integration for the ch.f., which consists of two steps. The first step is to evaluate the integrand over the quadrature points of the selected numerical integration method. It is a task that requires pricing all the cash flows at each quadrature point, and thus, depends on the number of trades. The second step is the summation of the cash flow prices over the quadrature points, which is done by an algorithm independent of the number of trades (e.g., Fast Fourier Transform (FFT) in the Clenshaw-Curtis quadrature method). Thus, we can focus on analyzing the complexity of the first step.

A feature of the credit exposure of linear products is that each cash flow leg involves a single currency. This holds for various financial instruments like IR swaps, FX forwards and swaps, cross-currency swaps, and others (including some simple nonlinear products as well). Suppose we have a portfolio of trades with N_d cash flow legs in the domestic currency, N_f cash flow legs in the foreign currency, and use N_{quad} quadrature points for each risk factor (in total N_{quad}^3 for the Hull-White-GBM model). The valuation of the domestic and foreign legs in their own currencies follows an order of $\mathcal{O}(N_d N_{quad})$ and $\mathcal{O}(N_f N_{quad}^2)$, respectively. Hence, the computational effort is determined by the valuation of the dominating foreign currency leg.

Subsequently, we aggregate all valuations in the foreign currency per quadrature point and convert the summed values from foreign to domestic currency. With the quadrature grid, the currency conversion is equivalent to an inner product of two tensors with a size of N_{quad}^3 and is independent of N_f . Thus, ignoring the simple arithmetic computation such as summation, the COS method requires to call the pricing functions at an order of $\mathcal{O}(N_f N_{quad}^2)$ times. In contrast, the number of calls to the pricing functions in MC methods is $(N_d + N_f)N_{sim}$ since MC methods must value all cash flow legs for each of the N_{sim} simulation scenarios. Given that $N_{sim} \gg N_{quad}^2$, the COS method significantly reduces the required number of pricing functions calls. This clarifies why the COS method avoids the “computational curse of large portfolios” seen in MC methods.

5 Theoretical error analysis

The errors in the COS-recovered CDF of the exposure, both at the netting-set level (13 and 15) and at the counterparty level (16), can be classified into two types: the truncation error stemming from the truncated Fourier series expansion; and other errors arising from the approximation of the true Fourier coefficients on $[a, b]$.

First, let us discuss the truncation error resulting from truncating the Fourier series expansion. This error shall dominate the error convergence when we suppress the approximation errors in the Fourier coefficients to a sufficiently low level.

The truncation error of the Fourier series expansion for the exposure distribution of a netting set converges exponentially, as long as the density function of the total MtM price V_t belongs to $\mathbb{C}^\infty([a, b])$ with nonzero derivatives. This is true in our considered case, because the MtM prices of the IR and FX linear products can be written as a linear combination of ZCBs with some FX adjustments, and the ZCBs and FX rates under the Hull–White–GBM model follow a log-normal distribution.

In details, the truncation error of the Fourier series expansion, denoted by ϵ_1 , can be expressed as

$$\epsilon_1 = \sum_{k=K+1}^{\infty} A_k \frac{b-a}{k\pi} \sin\left(k\pi \frac{e-a}{b-a}\right). \quad (22)$$

Due to Lemma 4.2 in [2], ϵ_1 can be bounded in a straightforward way. Inserting $V_k = \frac{b-a}{k\pi} \sin\left(k\pi \frac{e-a}{b-a}\right)$ into their derivations immediately yields the following:

Lemma 1. *Error ϵ_1 converges exponentially if the density function of the MtM price V_t belongs to $\mathbb{C}^\infty([a, b])$ with nonzero derivatives:*

$$|\epsilon_1| < P \exp(-K\nu), \quad (23)$$

where $\nu > 0$ is a constant, and P is a positive term that varies less than exponentially with the number of Fourier terms K .

The series truncation error for the exposure distribution at counterparty level converges with an algebraic rate. For a piecewise smooth function such as the exposure CDF at counterparty level, the convergence rate of a filtered Fourier series expansion depends on the order of the spectral filter. We formulate the lemma below based on the results of [20] and [8]:

Lemma 2. *If $F_t^c(\cdot)$, i.e., the true CDF of the counterparty level exposure E_t^c , is continuous at e , the difference between $F_{t,\text{cos}}^c(e)$ given in 16 and $F_t^c(e)$ converges as follows:*

$$|F_{t,\text{cos}}^c(e) - F_t^c(e)| \sim \mathcal{O}(K^{1-p}),$$

where K is the number of Fourier series terms, and p is the order of the spectral filter.

Second, the approximation errors of the Fourier coefficients can be reduced to an arbitrarily small level, if we use a sufficiently wide range $[a, b]$, and ensure a high level of accuracy in the ch.f. evaluated by the Clenshaw–Curtis quadrature.

The detailed analyses of the approximation errors in the Fourier coefficients can be found in A. Let ϵ_2 denote the error of approximating C_k by F_k . ϵ_2 converges as follows:

$$\lim_{[a,b] \rightarrow \mathbb{D}} \epsilon_2 \rightarrow 0,$$

where \mathbb{D} refers to the support of the concerned distribution. That is, $\mathbb{D} = (-\infty, +\infty)$ for the MtM price of the portfolio $V(\mathbf{X}_t)$, and $\mathbb{D} = [0, +\infty)$ for the counterparty exposure E_t^c .

The error of approximating F_k by A_k , denoted by ϵ_3 , can be minimized as well by employing a large number of quadrature points over a wide integration range. Holding the number of Fourier expansion terms K and the integration range constant, the convergence rate of ϵ_3 with respect to the number of quadrature points is exponential for the exposure distribution at netting–set level and algebraic for the exposure distribution at the counterparty level.

It is evident now that the total error arising from the approximation of Fourier coefficients is bounded by $|\epsilon_2| + |\epsilon_3|$.

6 Numerical tests

This section includes results of the numerical tests, designed to verify the error convergence as theoretically described in 5 and to compare both the calculation speed and the accuracy between the COS method and MC simulation.

The numerical results use the same setup as in [16], where the domestic and foreign currencies are chosen to be USD and JPY, respectively. To this extent, we define the functions for the ZCB by $P_d^M(0, T) = \exp(-0.02T)$ and $P_f^M(0, T) = \exp(-0.05T)$. The other model parameters are

$$\sigma_d = 0.7\%, \sigma_f = 1.2\%, \sigma_X = 2\%, a_d = 1\%, a_f = 5\%, \mu_X = 0.8\%,$$

and

$$\rho_{df} = 25\%, \rho_{dX} = -15\%, \rho_{fX} = -15\%.$$

The initial FX rate USD/JPY is set to be 105. All the testing portfolios are generated using a Python script such that different linear derivatives (IR forward rate agreement, IR swap, FX forward, and cross currency swap) are created with a random currency (either JPY or USD), fixed rate, tenor and maturity.

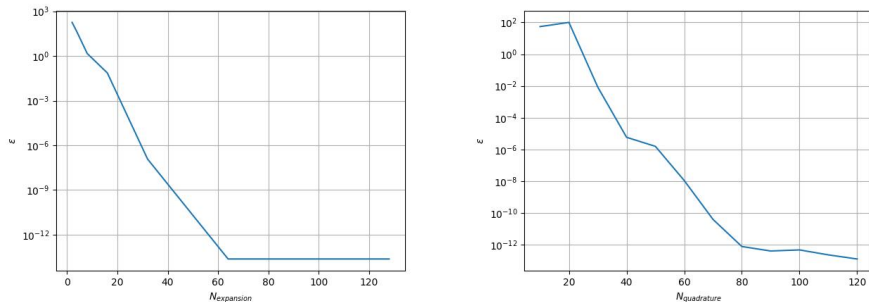
For all the experiments, the calculation speed is expressed in seconds and measured on a computer with an Intel Core i7-10700F CPU, 2.90GHz, with a cache size of 2048 KB.

6.1 Test results for PFE at the netting–set level

First, we embark on an examination of the convergence rate pertaining to the PFE at the netting–set level. Given the absence of an analytical solution, we

resort to the semi-analytical COS method for computing the reference PFE values. Notably, to achieve a high level of accuracy in the reference values, we employ rather stringent computation settings: 150 Fourier expansion terms, 130 quadrature points for each state variable, and the tolerance level TOL (for integration range truncation error) set to 10^{-12} .

The convergence is examined at $t = 7.4$ years, corresponding to half of the maximum maturity T_{\max} in the randomly generated portfolio. The expansion support is computed as detailed in 4.5. The reference values are compared with COS approximations with a varying number of expansion terms but a fixed number of quadrature points, and vice versa. The outcomes of the convergence analysis are presented in 1.



(a) Convergence of the PFE w.r.t the number of Fourier expansion terms. (b) Convergence of the PFE w.r.t the number of quadrature points.

Figure 1: Convergence of the PFE of a netting set containing 100 IR and FX derivatives. The error is expressed as a percentage of the benchmark PFE value \$3844.58, and plotted on a log scale.

1a confirms the theoretically predicted exponential convergence is observed, when the integration range truncation error (ϵ_2) is suppressed low enough via a small TOL and a large number of quadrature points. An error of machine precision with respect to the reference value is achieved with only 64 expansion terms. Similarly, 1b shows exponential convergence with respect to the number of quadrature points until the relative error is close to machine precision. This is expected for the Clenshaw–Curtis quadrature rule.

The computational time and accuracy of the netting-set level PFE calculations are compared between the MC simulation and the COS method. Three portfolios of different sizes are considered, i.e., consisting of 100, 1000 and 10000 derivatives. All derivatives of the 4 different contract types are put in the same netting set. The PFE is calculated for 20 equidistant exposure dates ranging from today’s date $t = 0$ until the maturity of the longest running derivative T_{\max} . The results of the COS method are generated using 32 expansion terms and 40 quadrature points per state variable. The time-averaged error is the difference between the reference PFE values and the PFE of the consid-

ered method, averaged over all time points. It is expressed as a percentage of the total notional at $t = 0$ of the corresponding portfolio. The total notional of the portfolios containing 100, 1000 and 10000 derivatives are, respectively, \$154,166.80, \$1,489,954.54 and \$15,170,624.49.

Table 1: Accuracy and computational time required to calculate the PFE of a netting set with 100 derivatives. The error is averaged over the 20 exposure dates and is expressed as a percentage of the total notional.

Method	CPU Time (Seconds)	Time-averaged Error (%)
MC ($0.5 \cdot 10^6$)	50.6	0.014
MC (10^6)	100.9	0.014
MC ($2 \cdot 10^6$)	200.8	0.015
COS	2.6	$5 \cdot 10^{-6}$

Table 2: Accuracy and computational time required to calculate the PFE of a netting with 1000 derivatives. The error is averaged over the 20 exposure dates and is expressed as a percentage of the total notional.

Method	CPU Time (Seconds)	Time-averaged Error (%)
MC ($0.5 \cdot 10^6$)	367.2	0.007
MC (10^6)	7,30.6	0.007
MC ($2 \cdot 10^6$)	1,459.2	0.007
COS	5.3	$5 \cdot 10^{-6}$

Table 3: Accuracy and computational time required to calculate the PFE of a netting set with 10,000 derivatives. The error is averaged over the 20 exposure dates and is expressed as a percentage of the total notional.

Method	CPU Time (Seconds)	Time-averaged Error (%)
MC ($0.5 \cdot 10^6$)	3501.8	0.005
MC (10^6)	6960.3	0.005
MC ($2 \cdot 10^6$)	13,886.7	0.005
COS	32.1	$2 \cdot 10^{-6}$

The test results verify the claim made in 4.6, that unlike MC, the COS method is free of the “computational curse of large portfolios”. The computational time of the MC simulation increases by one order of magnitude when the number of trades in the portfolio is increased by one order, as shown in 1, 2, and 3. The computational time of the COS method, however, marginally increases as the size of the portfolio grows. The extra time cost by the COS method is very limited, because the number of pricing function calls in COS is significantly less than that in MC.

Moreover, 1, 2, and 3 reveal that there is no apparent convergence for the number of MC simulations increasing from $0.5 \cdot 10^6$ to $2 \cdot 10^6$. For a risk metric

far into the tail of the distribution, there are fewer exposure paths, and thus, MC converges much slower here. The obtained results demonstrate the superior speed and accuracy of the COS method across all the evaluated portfolios. To achieve the same level of precision as the COS method using the MC approach would necessitate a significantly higher number of simulations, consequently leading to unbearably prolonged computational times.

6.2 Test results for PFE at the counterparty level

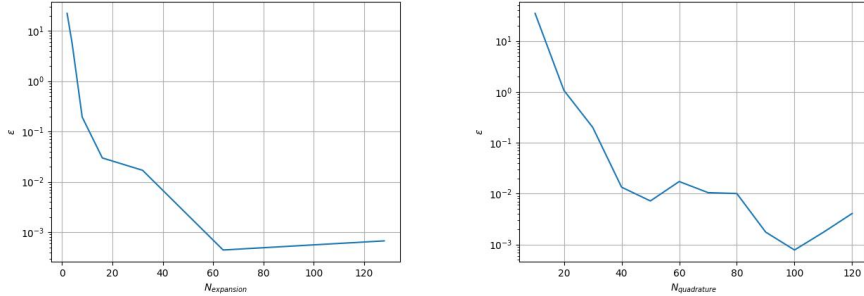
Here the efficiency and convergence of the counterparty level exposure are examined, using the same portfolio as discussed for the netting-set level tests. The portfolio is then divided into netting sets, each containing one contract type. The exposures of these individual netting sets are then grossed, i.e. aggregated without any netting or offsetting between the netting sets. Since we directly apply the Fourier series expansion to the summation of the exposures, a spectral filter is used to reduce the Gibbs phenomenon. We use an exponential filter with $p = 2$ from [8], i.e. $\sigma(\eta) = \exp(-\alpha\eta^p)$ where p must be even, $\alpha = -\log \epsilon_m$, and ϵ_m is the machine precision.

Remark 4. *The exponential filter of order 2 is chosen as low-order filtering is “desirable close to a discontinuity, because higher p values then give rise to a highly oscillatory filtered function” (quoted from [8]). A highly oscillatory filtered function could pose challenges when using root-finding algorithms at the 97.5% quantile level to obtain the PFE.*

The rate of convergence for the PFE pertaining to the counterparty level exposure is investigated under a configuration comparable to the netting-set level analysis. The reference PFE values are generated using the COS method, again with cautious parameter specifications of 150 expansion terms, 130 quadrature points for each state variable, and the tolerance level TOL for the integration range truncation error set at 10^{-12} .

Once more, the convergence is analysed at $t = T_{\max}/2 = 7.4$ years. The expansion support is determined following the procedure outlined in 4.5. The reference values are compared with COS approximations based on a varying number of expansion terms but a fixed number of quadrature points, and vice versa. The outcomes of the convergence analysis are presented in 2.

In 2a, we can observe the anticipated algebraic convergence when suppressing the integration range truncation error through a small TOL and an ample number of quadrature points. Notably, the rate of convergence in this scenario is markedly slower compared to that observed for netting-set level results, which benefits from the problem transformation that eliminates the floor constraint at 0. Despite this, the accuracy remains above 0.001% of the reference PFE value. 2b demonstrates gradual and somewhat irregular convergence of the error with respect to the number of quadrature points for the discontinuous integrand. It is noteworthy that the convergence trajectory appears non-monotonic. An explanation is that the amplitude of oscillation increases due to the slow convergence



(a) Convergence of the PFE w.r.t the number of Fourier expansion terms. (b) Convergence of the PFE w.r.t the number of quadrature points.

Figure 2: Convergence of the PFE for the counterparty level exposure in a portfolio containing 100 IR and FX derivatives. The error is expressed as a percentage of the benchmark PFE value \$4542.99 and plotted on a log scale.

in the presence of Gibbs phenomenon, which introduces perturbations affecting PFE outcomes obtained using the Newton–Raphson method.

We proceed by comparing the computational speed and accuracy between the MC simulation and the COS method. Once more, we assess three portfolios of varying sizes: comprising 100, 1000, and 10000 derivatives. The PFE calculations are performed at 20 equidistant exposure dates spanning from the present moment $t = 0$ to the maturity date T_{\max} of the longest-running derivative. The reference PFEs are evaluated via the COS method, based on 150 expansion terms and 130 quadrature points per state variable. In contrast, for performance comparison, the COS method outcomes are obtained using 32 expansion terms and 40 quadrature points per state variable. The time-averaged error is defined as the disparity between the reference PFE results and the tested approaches, expressed as a percentage of the total notional value at $t = 0$ of the corresponding portfolio. The total notional values for the portfolios encompassing 100, 1000, and 10000 derivatives are, sequentially, \$154,166.80, \$1,489,954.54, and \$15,170,624.49.

Table 4: The accuracy and computational time required to calculate the PFE of a counterparty portfolio with 100 derivatives. The error is averaged over the 20 exposure dates and is expressed as a percentage of the total notional.

Method	CPU Time (Seconds)	Time-averaged Error (%)
MC ($0.5 \cdot 10^6$)	51.2	0.017
MC (10^6)	101.6	0.018
MC ($2 \cdot 10^6$)	204.0	0.019
COS	2.7	0.008

Table 5: Accuracy and computational time required to calculate the PFE of a counterparty portfolio with 1000 derivatives. The error is averaged over the 20 exposure dates and is expressed as a percentage of the total notional.

Method	CPU Time (Seconds)	Time-averaged Error (%)
MC ($0.5 \cdot 10^6$)	377.9	0.009
MC (10^6)	737.5	0.008
MC ($2 \cdot 10^6$)	1,473.3	0.009
COS	5.3	0.001

Table 6: Accuracy and computational time required to calculate the PFE of a counterparty portfolio with 10,000 derivatives. The error is averaged over the 20 exposure dates and is expressed as a percentage of the total notional.

Method	CPU Time (Seconds)	Time-averaged Error (%)
MC ($0.5 \cdot 10^6$)	3,519.5	0.006
MC (10^6)	6,998.7	0.006
MC ($2 \cdot 10^6$)	14,097.4	0.006
COS	32.5	0.001

The computation to recover the CDF for counterparty level exposure involves multiplying Fourier coefficients by a spectral filter. This step barely adds computational time, as indicated by negligible differences in computation time compared to the netting-set level result. 4, 5 and 6 show that, again, the COS method is not subject to the “computational curse of large portfolios” as MC method.

Compared to netting-set level results, we observe an increase in the time-averaged error expressed as a percentage of the total notional by more than one order of magnitude. Nevertheless, the COS method remains at least twice as accurate as the MC simulation, while being at least 7 times faster.

6.3 EE sensitivities

The netting-set level EE sensitivities are computed for a portfolio containing 100 derivatives across 20 equidistant exposure dates. The sensitivity of the domestic and foreign shifted short rate is calculated by adjusting the initial values by 1 basis point in absolute terms. Similarly, the sensitivity with respect to the FX spot rate is determined using a relative shift of 1% of the the initial FX rate. These calculations align with established industry practices as outlined in [15].

Following the previous approach, we gauge the computational time required for computing EE sensitivities across all time points. The reference values are computed using the COS method, again with 150 expansion terms and 130 quadrature points for each state variable. For each time step, the expansion truncation range is adaptively updated according to the methodology outlined in 4.5. The error is computed as the time-averaged difference between the

reference values and the values obtained from either method. The outcomes of the COS method are obtained using 32 expansion terms and 40 quadrature points per state variable. A comprehensive presentation of all CPU times and accuracy outcomes is provided in 7.

Table 7: Accuracy and computational time required to calculate EE sensitivities of a netting set with 100 derivatives. The error is averaged over the 20 exposure dates and is expressed as a percentage of the total notional.

Method	CPU Time (seconds)	Error (%)		
		$\frac{\partial EE}{\partial x_{d,0}}$	$\frac{\partial EE}{\partial x_{f,0}}$	$\frac{\partial EE}{\partial X_0}$
MC ($0.5 \cdot 10^6$)	102.5	0.015	0.099	0.003
MC (10^6)	202.6	0.014	0.098	0.003
MC ($2 \cdot 10^6$)	403.1	0.014	0.098	0.003
COS	4.2	$5 \cdot 10^{-5}$	$3 \cdot 10^{-6}$	$6 \cdot 10^{-7}$

7 reports a single CPU time for all the sensitivities due to the equal computational complexity involved in their calculations. Additionally, the findings reaffirm the advantage of the COS method in terms of more than 20 times reduced computational time, coupled with the attainment of a significantly diminished time-averaged error, when compared to MC.

In comparison to the PFE results, the computational time required by the MC method is roughly doubled. The MC simulation necessitates an additional path to be generated for shocking the state variable, and the portfolio's exposure needs to be calculated twice to determine the sensitivity. Similarly, the COS method requires the portfolio's exposure to be evaluated twice since the shock-and-revalue method is employed.

Remark 5. *By definition of the EE, we can calculate the sensitivities of each netting set separately and then take the sum of these sensitivities to get the counterparty level EE sensitivities. Since we can omit the flooring of netting-set level calculations as explained earlier, fewer quadrature points and expansion terms are needed for a higher accuracy and lower CPU time than directly applying the shock-and-revalue approximation to the counterparty level exposure.*

7 Conclusions

The paper introduces a novel approach for calculating CCR measures and associated sensitivities using the Fourier-cosine expansion, extending the COS method from option pricing to the realm of CCR quantification. The goal is to provide a fast and accurate method for practical CCR assessments on a portfolio level.

The COS method is applicable whenever the joint density function of the risk factors is known or numerically solvable and when the valuation of each financial product in the portfolio concerns a moderate number of risk factors.

The pronounced advantage of the COS method is its efficiency especially in handling large portfolios. It considerably outperforms the industry-standard Monte Carlo method. In numerical tests with real-sized portfolios, the COS method demonstrates significantly higher accuracy (several orders of magnitude more accurate) and faster computational speed (at least 20 times) compared to MC. Theoretical error analyses further prove its stability and convergence. These results suggest that the COS method is a promising alternative for efficient counterparty credit risk quantification, especially for portfolios with relatively few risk factors.

A limitation of this method is that the required numerical integration for the characteristic function of the portfolio-level exposure becomes computationally expensive when more risk factors are added. The “curse of dimensionality”, together with the inclusion of collaterals, shall be addressed in a follow-up paper, where we combine efficient dimension-reduction techniques with the COS method.

A Approximation errors in the Fourier coefficients

Three distinct sources of errors manifest in the approximation of the Fourier coefficients. The initial error originates from the COS truncation range $[a, b]$, leading to deviations between C_k and F_k . The remaining two errors emerge from the application of Clenshaw–Curtis quadrature rule to numerically integrate the ch.f, leading to deviations between F_k and A_k . There the errors arise from the approximation of an integral using quadrature points, coupled with the necessity to truncate the integral’s infinite domain. The latter two errors are hereafter grouped together and referred to as the numeric integration error. Our central emphasis in this section is directed towards the propagation of these errors throughout the Fourier series expansion.

In the discussion here, we fix the number of the Fourier expansion terms K . We denote ϵ_2 as the error in the CDF due to the difference between F_k and C_k , and ϵ_3 as the error due to the difference between A_k and F_k . Because $|A_k - C_k| \leq |F_k - C_k| + |A_k - F_k|$, the total error due to the approximations in the Fourier coefficients is less than $|\epsilon_2| + |\epsilon_3|$. Below, we give the bounds of ϵ_2 and ϵ_3 separately.

Lemma 3. *Denote the density function of the portfolio value V_t by f . Without loss of generality we assume that f is bounded with finite first and second moments. The error ϵ_2 due to the COS truncation range $[a, b]$ can be bounded as*

$$\lim_{[a,b] \rightarrow \mathbb{D}} \epsilon_2 \rightarrow 0, \quad (24)$$

where \mathbb{D} refers to the support of the concerned distribution. That is, $\mathbb{D} = (-\infty, +\infty)$ for the MtM price of the portfolio $V(\mathbf{X}_t)$, and $\mathbb{D} = [0, +\infty)$ for the counterparty exposure E_t^c .

Proof. $F_k - C_k = \frac{2}{b-a} \int_{\mathbb{D} \setminus [a,b]} \cos \frac{k\pi(v-a)}{b-a} f(v) dv$. Thus at netting set level, ϵ_2 in the CDF $F_{t,cos}^n(t)$ is of the form

$$\epsilon_2 = \frac{e-a}{b-a} \int_{\mathbb{D} \setminus [a,b]} f(v) dv + \sum_{k=1}^K \frac{2}{k\pi} \sin \frac{k\pi(e-a)}{b-a} \int_{\mathbb{D} \setminus [a,b]} \cos \frac{k\pi(v-a)}{b-a} f(v) dv.$$

The leading term $\frac{e-a}{b-a} \int_{\mathbb{D} \setminus [a,b]} f(v) dv$ converges to 0, as the COS truncation range $[a, b]$ grows to cover the entire \mathbb{D} .

And the Cauchy–Schwarz inequality gives an bound of the series summation $\sum_{k=1}^K \frac{2}{k\pi} \sin \frac{k\pi(e-a)}{b-a} \int_{\mathbb{D} \setminus [a,b]} \cos \frac{k\pi(v-a)}{b-a} f(v) dv$ as below

$$\frac{2}{\pi} \sqrt{\sum_{k=1}^K \frac{1}{k^2} \sin^2 \frac{k\pi(e-a)}{b-a}} \sqrt{\sum_{k=1}^K c_k^2},$$

where $c_k = \int_{\mathbb{D} \setminus [a,b]} \cos \frac{k\pi(v-a)}{b-a} f(v) dv$.

Note that $\sum_{k=1}^N \frac{1}{k^2} \sin^2 \frac{k\pi(e-a)}{b-a}$ is bounded by $\frac{\pi^2}{6}$.

Under the assumption that the probability density f is bounded with finite first and second moments, $\sum_{k=1}^N c_k^2 \rightarrow 0$ as $\lim_{[a,b] \rightarrow \mathbb{D}}$ (see [9]). Thus we can make ϵ_2 arbitrarily small if the COS truncation range $[a, b]$ is sufficiently wide.

At counterparty level, ϵ_2 in the CDF $F_{t,\text{cos}}^c(t)$ is of the form

$$\epsilon_2 = \frac{e-a}{b-a} \int_{\mathbb{D} \setminus [a,b]} f(v) dv + \sum_{k=1}^K \frac{2}{k\pi} \sigma(k/K) \sin \frac{k\pi(e-a)}{b-a} \int_{\mathbb{D} \setminus [a,b]} \cos \frac{k\pi(v-a)}{b-a} f(v) dv.$$

Note that $\sigma(k/K) \leq 1$, implying $\sum_{k=1}^K \frac{1}{k^2} \sigma(k/K)^2 \sin^2 \frac{k\pi(e-a)}{b-a} \leq \frac{\pi^2}{6}$ as well. Thus the same arguments that are applied to the netting set level can be repeated to bound ϵ_2 at counterparty level. \square

Finally, we briefly remark on the error ϵ_3 due to evaluating the ch.f. by the Clenshaw–Curtis quadrature method. Let $F_k = A_k + \epsilon(J, \text{TOL}, k)$, where J is the number of quadrature points adopted in the Clenshaw–Curtis quadrature rule, TOL is a chosen tolerance of error of the integration range defined in the 4.1, and $\epsilon(J, \text{TOL}, k)$ denotes the Clenshaw–Curtis error in A_k . In general, if we use a large amount of quadrature points and a wide enough integration range, we can guarantee the accuracy of each A_k .

Specifically, let us consider fixing the integration range (thus given TOL). For the exposure distribution at the netting–set level, if the integrand for the ch.f., i.e., $e^{i\omega V(\mathbf{X}_t)} f(\mathbf{X}_t)$, has an analytical extension to the complex plane for each integration dimension, the Clenshaw–Curtis method shall converge exponentially with respect to the number of the quadrature points. For example, this condition holds for the Hull–White–GBM model with linear IR and FX products, because there V is a linear combination of exponential functions, and f is the Gaussian density. Moreover, since the integrands for different k are uniformly bounded, i.e., $|e^{i\omega V(\mathbf{X}_t)} f(\mathbf{X}_t)| \leq f(\mathbf{X}_t)$ for all $\omega = k\pi/(b-a)$, $k \geq 0$, the Clenshaw–Curtis errors for $\{A_{k,0 \leq k \leq K}\}$ can be bounded uniformly (see e.g., Equation 10 in [17]). In this case, we have the following statement for ϵ_3 :

Lemma 4. *If $\epsilon(J, \text{TOL}, k)$ are uniformly bounded by $\epsilon(J, \text{TOL})$, then ϵ_3 in the CDF of the exposure at netting set level converges as*

$$\epsilon_3 \sim \mathcal{O}(\sqrt{K}) \cdot \epsilon(J, \text{TOL}), \quad (25)$$

Proof.

$$\begin{aligned} \epsilon_3 &= \left| \frac{\epsilon(J, \text{TOL}, 0)}{2} (e-a) + \sum_{k=1}^K \epsilon(J, \text{TOL}, k) \frac{b-a}{k\pi} \sin \left(k\pi \frac{e-a}{b-a} \right) \right| \\ &\leq \left((K+1)\epsilon(J, \text{TOL})^2 \left(\frac{(e-a)^2}{4} + \sum_{k=1}^K \frac{(b-a)^2}{k^2 \pi^2} \sin^2 \left(k\pi \frac{e-a}{b-a} \right) \right) \right)^{\frac{1}{2}} \\ &\leq \left((K+1)\epsilon(J, \text{TOL})^2 \left(\frac{(e-a)^2}{4} + \frac{(b-a)^2}{\pi^2} \sum_{k=1}^K \frac{1}{k^2} \right) \right)^{\frac{1}{2}}, \end{aligned}$$

Since $\sum_{k=1}^N \frac{1}{k^2} < \frac{\pi^2}{6}$, we have $\epsilon_3 \sim \mathcal{O}(\sqrt{K}) \cdot \epsilon(J, \text{TOL})$. \square

Note that for the exposure distribution at the counterparty level, the integrand, i.e., $e^{i\omega \max(V(\mathbf{X}_t), 0)} f(\mathbf{X}_t)$ does not admit a continuous first-order derivative. As a result, Clenshaw–Curtis does not have an exponential convergence rate with respect to the number of quadrature points. Instead, the convergence rate with respect to the number of quadrature points is algebraic. We cannot directly use the error estimates of the Clenshaw–Curtis method in the literature, which typically assume stronger smooth condition, to obtain an uniform bound $\epsilon(J, \text{TOL}, k)$. However, by fixing the number of Fourier expansion terms K , we can still guarantee the error convergence for the first K leading Fourier coefficients.

References

- [1] M. DI FRANCESCO, *A general gaussian interest rate model consistent with the current term structure*, International Scholarly Research Notices, (2012), <https://doi.org/10.5402/2012/673607>.
- [2] F. FANG AND C. W. OOSTERLEE, *A novel pricing method for european options based on fourier-cosine series expansions*, SIAM Journal on Scientific Computing, 31 (2009), pp. 826–848, <https://doi.org/10.1137/080718061>.
- [3] R. FENG AND P. LI, *Sample recycling method—a new approach to efficient nested monte carlo simulations*, Insurance: Mathematics and Economics, 105 (2022), pp. 336–359, <https://doi.org/10.1016/j.insmatheco.2022.04.012>.
- [4] P. GLASSERMAN, P. HEIDELBERGER, AND P. SHAHABUDDIN, *Importance sampling and stratification for value-at-risk*, vol. 1, December 1999, <https://doi.org/10.1145/324138.324241>.
- [5] K. GLAU, R. PACHON, AND C. PÖTZ, *Speed-up credit exposure calculations for pricing and risk management*, Quantitative Finance, 21 (2021), pp. 481–499, <https://doi.org/10.1080/14697688.2020.1781236>.
- [6] K. GLAU AND L. WUNDERLICH, *Neural network expression rates and applications of the deep parametric pde method in counterparty credit risk*, Annals of Operations Research, (2023), pp. 1–27, <https://doi.org/10.1007/s10479-023-05315-4>.
- [7] A. GNOATTO, A. PICARELLI, AND C. REISINGER, *Deep xva solver: A neural network-based counterparty credit risk management framework*, SIAM Journal on Financial Mathematics, 14 (2023), pp. 314–352, <https://doi.org/10.1137/21M1457606>.

- [8] D. GOTTLIEB AND C.-W. SHU, *On the gibbs phenomenon and its resolution*, SIAM review, 39 (1997), pp. 644–668, <https://doi.org/10.1137/S0036144596301390>.
- [9] G. JUNIKE AND K. PANKRASHKIN, *Precise option pricing by the cos method - how to choose the truncation range*, Applied Mathematics and Computation, 421 (2022), <https://doi.org/10.1016/j.amc.2022.126935>.
- [10] P. KARLSSON, S. JAIN, AND C. W. OOSTERLEE, *Counterparty credit exposures for interest rate derivatives using the stochastic grid bundling method*, Applied Mathematical Finance, 23 (2016), pp. 175–196, <https://doi.org/10.1080/1350486X.2016.1226144>.
- [11] S. LI, C. PENG, Y. BAO, AND Y. ZHAO, *Explicit expressions to counterparty credit exposures for forward and european option*, The North American Journal of Economics and Finance, 52 (2020), p. 101130, <https://doi.org/10.1016/j.najef.2019.101130>.
- [12] S. LI, C. PENG, Y. BAO, Y.-L. ZHAO, AND Z. CAO, *Analytical expressions to counterparty credit risk exposures for interest rate derivatives*, Acta Mathematicae Applicatae Sinica, English Series, 38 (2022), pp. 254–270, <https://doi.org/10.1007/s10255-022-1074-8>.
- [13] X. S. LIN AND S. YANG, *Fast and efficient nested simulation for large variable annuity portfolios: A surrogate modeling approach*, Insurance: Mathematics and Economics, 91 (2020), pp. 85–103, <https://doi.org/10.1016/j.insmathco.2020.01.002>.
- [14] S. NATENBERG, *Option Volatility Trading Strategies*, John Wiley & Sons, 2012.
- [15] B. C. ON BANKING SUPERVISION, *Consultative document, credit valuation adjustment risk: targeted final revisions*, 2019, www.bis.org.
- [16] V. PITERBARG, *A multi-currency model with fx volatility skew*, 2005, <https://doi.org/10.2139/ssrn.685084>.
- [17] R.D.RIESS AND L.W.JOHNSON, *Error estimates for clenshaw-curtis quadrature*, Numerische Mathematik, 18 (1971), pp. 345 – 353, <https://doi.org/10.1007/BF01404685>.
- [18] M. RUIJTER, M. VERSTEEGH, AND C. W. OOSTERLEE, *On the application of spectral filters in a fourier option pricing technique*, Journal of Computational Finance, 19 (2015), pp. 75–106, <https://doi.org/10.21314/JCF.2015.306>.
- [19] Y. T. TRINH AND B. HANZON, *Option pricing and cva calculations using the monte carlo-tree (mc-tree) method*, arXiv, (2022), <https://doi.org/10.48550/arXiv.2202.00785>.

- [20] H. VANDEVEN, *Family of spectral filters for discontinuous problems*, Journal of Scientific Computing, 6 (1991), pp. 159 – 191, <https://doi.org/10.1007/BF01062118>.